J|A|C|S
ARTICLES
Published on Web 10/05/2007

Polarized X-ray Absorption Spectroscopy of Single-Crystal Mn(V) Complexes Relevant to the Oxygen-Evolving Complex of Photosystem II

Junko Yano,*[,†] John Robblee,[†,‡,⊥] Yulia Pushkar,[†,‡] Matthew A. Marcus,[§] Jesper Bendix,[¶] José M. Workman,[£,#] Terrence J. Collins,[£] Edward I. Solomon,[@] Serena DeBeer George,*[,||] and Vittal K. Yachandra[†]

Contribution from the Physical Biosciences Division, Lawrence Berkeley National Laboratory, Berkeley, California 94720, Department of Chemistry, University of California, Berkeley, California 94720-5230, Advanced Light Source, Lawrence Berkeley National Laboratory, Berkeley, California 94720, Department of Chemistry, University of Copenhagen, Universitetsparken 5, DK-2100, Denmark, Department of Chemistry, Carnegie Mellon University, Pittsburgh, Pennsylvania 15213, Department of Chemistry, Stanford University, Stanford, California 94305, and Stanford Synchrotron Radiation Laboratory, SLAC, Stanford University, Stanford, California 94309

Received February 22, 2007; E-mail: jyano@lbl.gov; debeer@stanford.edu

Abstract: High-valent Mn-oxo species have been suggested to have a catalytically important role in the water splitting reaction which occurs in the Photosystem II membrane protein. In this study, five- and six-coordinate mononuclear Mn(V) compounds were investigated by polarized X-ray absorption spectroscopy in order to understand the electronic structure and spectroscopic characteristics of high-valent Mn species. Single crystals of the Mn(V)-nitrido and Mn(V)-oxo compounds were aligned along selected molecular vectors with respect to the X-ray polarization vector using X-ray diffraction. The local electronic structure of the metal site was then studied by measuring the polarization dependence of X-ray absorption near-edge spectroscopy (XANES) pre-edge spectra (1s to 3d transition) and comparing with the results of density functional theory (DFT) calculations. The Mn(V)-nitrido compound, in which the manganese is coordinated in a tetragonally distorted octahedral environment, showed a single dominant pre-edge peak along the Mn≡N axis that can be assigned to a strong $3d_{z^2}-4p_z$ mixing mechanism. In the square pyramidal Mn-(V)-oxo system, on the other hand, an additional peak was observed at 1 eV below the main pre-edge peak. This component was interpreted as a 1s to $3d_{xz,yz}$ transition with $4p_{x,y}$ mixing, due to the displacement of the Mn atom out of the equatorial plane. The XANES results have been correlated to DFT calculations, and the spectra have been simulated using a TD (time-dependent)-DFT approach. The relevance of these results to understanding the mechanism of the photosynthetic water oxidation is discussed.

Introduction

Mn complexes play critical roles in the fundamental chemical reactions in many biological systems. Perhaps the most important reaction is the oxidation of water to oxygen by the photosynthetic membrane protein (Photosystem II), present in green plants, algae, and cyanobacteria. This process is catalyzed by a Mn_4Ca cluster and takes place in the oxygen-evolving complex (OEC) in PS II.[1−6] The OEC couples the one-electron primary charge separation (photo-oxidation) occurring at the PS II reaction center with the four-electron water oxidation chemistry. During this process, the OEC cycles through five intermediate S states, S_0-S_4, storing oxidative equivalents serially until it reaches the S_4 state.[7] The formal oxidation states of S_1 and S_2 are generally accepted as $Mn_4(III_2,IV_2)$ and $Mn_4(III,IV_3)$.[8−10] Some conflict remains in the assignment of oxidation states in S_0 and S_3.[10−13] The S_0 state is considered to be either $Mn_4(III_3,IV)$ or $Mn_4(II,III_2,IV)$. In the S_2 to S_3

† Physical Biosciences Division, Lawrence Berkeley National Laboratory.
‡ University of California, Berkeley.
§ Advanced Light Source, Lawrence Berkeley National Laboratory.
¶ University of Copenhagen.
£ Carnegie Mellon University.
@ Department of Chemistry, Stanford University.
|| SLAC, Stanford University.
⊥ Current address: Momenta Pharmaceuticals, 675 W Kendall St., Cambridge, MA 02142-1110.
Current address: Centre College, Danville, KY 40422.

(1) Britt, R. D.; Peloquin, J. M.; Campbell, K. A. *Annu. Rev. Biophys. Biomol. Struct.* **2000**, *29*, 463−495.
(2) Diner, B. A.; Rappaport, F. *Annu. Rev. Plant Biol.* **2002**, *53*, 551−580.
(3) McEvoy, J. P.; Brudvig, G. W. *Chem. Rev.* **2006**, *106*, 4455−4483.
(4) Ferreira, K. N.; Iverson, T. M.; Maghlaoui, K.; Barber, J.; Iwata, S. *Science* **2004**, *303*, 1831−1838.
(5) Loll, B.; Kern, J.; Saenger, W.; Zouni, A.; Biesiadka, J. *Nature* **2005**, *438*, 1040−1044.
(6) Yano, J.; Kern, J.; Sauer, K.; Latimer, M.; Pushkar, Y.; Biesiadka, J.; Loll, B.; Saenger, W.; Messinger, J.; Zouni, A.; Yachandra, V. K. *Science* **2006**, *314*, 821−825.
(7) Kok, B.; Forbush, B.; McGloin, M. *Photochem. Photobiol.* **1970**, *11*, 457−476.
(8) Yamauchi, T.; Mino, H.; Matsukawa, T.; Kawamori, A.; Ono, T. *Biochemistry* **1997**, *36*, 7520−7526.
(9) Campbell, K. A.; Peloquin, J. M.; Pham, D. P.; Debus, R. J.; Britt, R. D. *J. Am. Chem. Soc.* **1998**, *120*, 447−448.

transition, whether a Mn-centered oxidation state change occurs or whether a ligand-centered oxidation state change takes place has been an open question. The final S_4 state is assumed to oxidize two substrate water molecules to dioxygen, returning to the S_0 state. The S_4 state remained undetected until recent studies showed that a candidate for this state or intermediate states prior to the S_4 state could be detected experimentally. A study by Clausen et al. has shown evidence for an intermediate state between the S_3 and S_0 states generated under high O_2 pressure.[14] A subsequent study by Haumann et al. has also captured an intermediate state by using time-resolved X-ray absorption spectroscopy.[15] Although whether the intermediate state(s) observed in these studies is(are) actually the S_4 state or not has been discussed,[3] these findings have opened the door for more detailed study of the mechanism of water oxidation.

On the basis of the many possible Mn_4Ca structures consistent with EPR, IR, and X-ray absorption spectroscopy, and more recently from crystallography, several oxygen-evolving mechanisms have been proposed.[16−18] Among these, one mechanism that has been widely discussed suggests the involvement of Mn(V)-oxo species in the final S_4 state. It is proposed that the electrophilic Mn(V)-oxo is a good candidate for a nucleophilic attack by water or hydroxide, bound either to Mn or Ca, to form an O−O bond.[19,20] Recently, Shimazaki et al. have reported a Mn(V)-oxo porphyrin dimer which evolves O_2, implicating the involvement of Mn(V) in a model system.[21] However, whether or not Mn(V)-oxo is involved in the catalytic process of PS II is a key question that needs to be answered in order to understand the mechanism of water oxidation.

In most cases, studies of oxidation states and electronic structures of the active site of metalloproteins are based on the knowledge of well-characterized model compounds[22−24] using spectroscopic techniques such as X-ray absorption spectroscopy and electron paramagnetic spectroscopy. In the case of Mn, however, most of the model compound studies have so far focused on the Mn(III) and Mn(IV) systems. Though many Mn(V) model complexes have been reported,[21,25−32] there have been relatively few detailed spectroscopic studies of Mn(V) complexes.[31,33]

The X-ray absorption near-edge spectra (XANES) have been used to derive information about the oxidation states and the environment surrounding Mn in inorganic compounds as well as in the OEC of PS II.[34] The spectra reflect the 1s to 4p (unoccupied valence orbitals) transition according to the dipole selection rules. The energy position of the absorption edge is therefore dependent on the effective charge density through core hole shielding effects of 1s orbitals. While the interpretation of the XANES region is often difficult due to the influence of many factors contributing to the spectral shape, the weak "pre-edge" peaks ~10 eV below the XANES region have been used to extract information about the electronic structure and the local symmetry at the metal site. The pre-edge peak is assigned formally to a dipole-forbidden 1s to 3d transition that gains intensity through distortion which eliminates the inversion symmetry and allows metal 4p orbital mixing into the 3d final state.[35,36]

In general, pre-edge peaks are less resolved in isotropic solution or powder samples. Their interpretation is also associated with a large uncertainty because of a strong background from dipole-allowed transitions at higher energies. One approach is to use polarized XAS of single crystals to orientationally resolve the contributing transitions.[37,38] This method allows us to selectively enhance specific transitions along certain molecular vectors through crystallographic alignment of molecules with respect to the incident X-ray polarization vector. Thus, one can relate the molecular orientation and spectral dichroism and make rigorous assignments of the pre-edge peaks. The plane-polarized nature of synchrotron radiation is ideally suited for polarized X-ray absorption spectroscopy.

Single-crystal X-ray spectroscopy has been performed on Cr═O porphyrin complexes, dithiomolybdate, and a series of Cu(II) model complexes.[39−42] The Cr═O complexes, for example, showed an intense 1s → 3d pre-edge transition when the incident light was polarized along the Cr═O bond.[41] This was interpreted by Templeton et al.[35,36] in a similar system as a transition between the metal 1s core level and an antibonding molecular

(10) Messinger, J.; Robblee, J. H.; Bergmann, U.; Fernandez, C.; Glatzel, P.; Visser, H.; Cinco, R. M.; McFarlane, K. L.; Bellacchio, E.; Pizarro, S. A.; Cramer, S. P.; Sauer, K.; Klein, M. P.; Yachandra, V. K. *J. Am. Chem. Soc.* **2001**, *123*, 7804−7820.
(11) Messinger, J.; Robblee, J. H.; Yu, W. O.; Sauer, K.; Yachandra, V. K.; Klein, M. P. *J. Am. Chem. Soc.* **1997**, *119*, 11349−11350.
(12) Dau, H.; Iuzzolino, L.; Dittmer, J. *Biochim. Biophys. Acta* **2001**, *1503*, 24−39.
(13) Boussac, A.; Sugiura, M.; Kirilovsky, D.; Rutherford, A. W. *Plant Cell Physiol.* **2005**, *46*, 837−842.
(14) Clausen, J.; Junge, W. *Nature* **2004**, *430*, 480−483.
(15) Haumann, M.; Liebisch, P.; Muller, C.; Barra, M.; Grabolle, M.; Dau, H. *Science* **2005**, *310*, 1019−1021.
(16) McEvoy, J. P.; Brudvig, G. W. *Phys. Chem. Chem. Phys.* **2004**, *6*, 4754−4763.
(17) Siegbahn, P. E. M. *Chem.−Eur. J.* **2006**, *12*, 9217−9227.
(18) Messinger, J. *Phys. Chem. Chem. Phys.* **2004**, *6*, 4764−4771.
(19) Pecoraro, V. L.; Hsieh, W.-Y. In *Manganese and Its Role in Biological Processes*; Sigel, A., Sigel, H., Eds.; Marcel Dekker Inc.: New York, 2000; Vol. 37, pp 429−504.
(20) Vrettos, J. S.; Brudvig, G. W. *Philos. Trans. R. Soc. London, Ser. B* **2002**, *357*, 1395−1404.
(21) Shimazaki, Y.; Nagano, T.; Takesue, H.; Ye, B. H.; Tani, F.; Naruta, Y. *Angew. Chem., Int. Ed.* **2004**, *43*, 98−100.
(22) Westre, T. E.; Kennepohl, P.; DeWitt, J. G.; Hedman, B.; Hodgson, K. O.; Solomon, E. I. *J. Am. Chem. Soc.* **1997**, *119*, 6297−6314.
(23) Roe, A. L.; Schneider, D. J.; Mayer, R. J.; Pyrz, J. W.; Widom, J.; Que, L., Jr. *J. Am. Chem. Soc.* **1984**, *106*, 1676−1681.
(24) Kau, L. S.; Spirasolomon, D. J.; Pennerhahn, J. E.; Hodgson, K. O.; Solomon, E. I. *J. Am. Chem. Soc.* **1987**, *109*, 6433−6442.
(25) Gross, Z.; Golubkov, G.; Simkhovich, L. *Angew. Chem., Int. Ed.* **2000**, *39*, 4045−4047.
(26) Groves, J. T.; Watanabe, Y.; McMurry, T. J. *J. Am. Chem. Soc.* **1983**, *105*, 4489−4490.
(27) Groves, J. T.; Takahashi, T. *J. Am. Chem. Soc.* **1983**, *105*, 2073−2074.
(28) MacDonnell, F. M.; Fackler, N. L. P.; Stern, C.; O'Halloran, T. V. *J. Am. Chem. Soc.* **1994**, *116*, 7431−7432.
(29) Mandimutsira, B. S.; Ramdhanie, B.; Todd, R. C.; Wang, H. L.; Zareba, A. A.; Czernuszewicz, R. S.; Goldberg, D. P. *J. Am. Chem. Soc.* **2002**, *124*, 15170−15171.
(30) Collins, T. J.; Powell, R. D.; Slebodnick, C.; Uffelman, E. S. *J. Am. Chem. Soc.* **1990**, *112*, 899−901.
(31) Song, W. J.; Seo, M. S.; DeBeer George, S.; Ohta, T.; Song, R.; Kang, M. J.; Tosha, T.; Kitagawa, T.; Solomon, E. I.; Nam, W. *J. Am. Chem. Soc.* **2007**, *129*, 1268−1277.
(32) Bendix, J.; Deeth, R. J.; Weyhermüller, T.; Bill, E.; Wieghardt, K. *Inorg. Chem.* **2000**, *39*, 930−938.
(33) Weng, T. C.; Hsieh, W. Y.; Uffelman, E. S.; Gordon-Wylie, S. W.; Collins, T. J.; Pecoraro, V. L.; Penner-Hahn, J. E. *J. Am. Chem. Soc.* **2004**, *126*, 8070−8071.
(34) Yachandra, V. K.; Sauer, K.; Klein, M. P. *Chem. Rev.* **1996**, *96*, 2927−2950.
(35) Templeton, D. H.; Templeton, L. K. *Acta Crystallogr.* **1980**, *A36*, 237−241.
(36) Templeton, D. H.; Templeton, L. K. *Acta Crystallogr.* **1982**, *A38*, 62−67.
(37) Pickering, I. J.; George, G. N. *Inorg. Chem.* **1995**, *34*, 3142−3152.
(38) Sauer, K.; Yano, J.; Yachandra, V. K. *Photosynth. Res.* **2005**, *85*, 73−86.
(39) Hahn, J. E.; Scott, R. A.; Hodgson, K. O.; Doniach, S.; Desjardins, S. R.; Solomon, E. I. *Chem. Phys. Lett.* **1982**, *88*, 595−598.
(40) Smith, T. A.; Penner-Hahn, J. E.; Berding, M. A.; Doniach, S.; Hodgson, K. O. *J. Am. Chem. Soc.* **1985**, *107*, 5945−5955.
(41) Penner-Hahn, J. E.; Benfatto, M.; Hedman, B.; Takahashi, T.; Doniach, S.; Groves, J. T.; Hodgson, K. O. *Inorg. Chem.* **1986**, *25*, 2255−2259.
(42) Shadle, S. E.; Penner-Hahn, J. E.; Schugar, H. J.; Hedman, B.; Hodgson, K. O.; Solomon, E. I. *J. Am. Chem. Soc.* **1993**, *115*, 767−776.

Scheme 1. Chemical Structures of Mn(V)-nitrido and Mn(V)-oxo Complexes

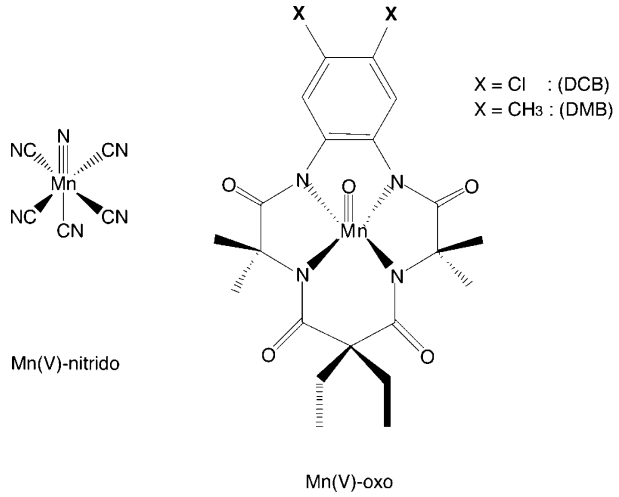

orbital with metal d_{z^2} and oxygen p_z character. However, as has been reported more recently,[43] the intense pre-edge peak formally results from metal $4p_z$ mixing with metal $3d_{z^2}$ orbitals, which originates from overlap of the ligand orbitals with both the metal 3d and 4p orbitals. Polarized spectroscopy has also been applied to protein crystals.[6,44,45]

We report here a detailed study of the polarized X-ray absorption spectroscopy of single crystals of two Mn(V) complexes: a Mn(V)-nitrido[32] (which is six-coordinate) and two Mn(V)-oxo complexes (which are five-coordinate, square pyramidal).[46] All of these complexes exhibited pronounced XANES dichroism which originate from the Mn(V)-nitrido and Mn(V)-oxo bonds. X-ray absorption spectroscopy and X-ray diffraction are combined to interpret the polarization characteristics of the spectra based on the molecular orientation. The experimental results are complemented by electronic structure calculations, which are used to obtain theoretical simulations of the experimental spectra. These results provide electronic structural insight into Mn(V)-oxo complexes and their possible contributions to reactivity.

Experimental Section

Samples. The Mn model complexes, $[Rh(en)_3][Mn(N)(CN)_5]\cdot H_2O$ (Mn(V)-nitrido) (en = 1,2-diaminoethane), and the macrocyclic Mn(V)-oxo complexes, Mn(V)-oxo(DCB) and Mn(V)-oxo(DMB) (Scheme 1), were synthesized and crystallized as described in the literature.[32,46] The structures of these compounds (Mn(V)-nitrido and Mn(V)-oxo(DCB)) have been characterized by X-ray diffraction. In both Mn(V)-nitrido and Mn(V)-oxo compounds, the local symmetry around Mn is approximately C_{4v}. The metal center is displaced out of the plane defined by the equatorial cyanide ligands toward the nitrido or oxo ligand, the displacement being 0.2 and 0.6 Å in Mn(V)-nitrido and Mn(V)-oxo(DCB), respectively.

Mn(V)-nitrido Single Crystal. The complex crystallizes in the space group $P6_3$, with six molecules per unit cell.[32] As shown in Figure 1a,b, the Mn-nitrido bond for each molecule in the unit cell is nearly collinear with the crystallographic *c*-axis (the angle between each Mn−N vector and the crystallographic *c*-axis is 9.4°). The long axis of the crystal was found to coincide with the crystallographic *c*-axis. The molecular axis was defined as shown in Figure 1c; the molecular *x*- and *y*-axes are in the equatorial plane along the metal−ligand bonds, and the *z*-axis is defined along the Mn−N bond.

Mn(V)-oxo Single Crystals. Among the two compounds, Mn(V)-oxo(DCB) and Mn(V)-oxo(DMB),[30] a crystal structure has been reported only for the former compound. The space group of the crystal is $P2_1$ with four molecules per unit cell. The Mn-oxo bond for each molecule in the unit cell is aligned approximately in the *ac*-plane of the crystal and is tilted about 27° from the *a*-axis (Figure 2a,b). In the *bc*-plane, the neighboring molecules are rotated about 90° from each other. The definition of the molecular axis used in this study is shown in Figure 2c. The molecular *x*- and *y*-axes are again in the equatorial plane along the metal−ligand bonds, and the *z*-axis is along the Mn−O bond.

Polarized X-ray Absorption Spectra Measurements. The crystals were mounted on a home-built two-circle goniometer. This fixture permits rotation around two perpendicular axes, ϕ and χ. The incoming X-ray beam is polarized along the laboratory *X*-axis. The laboratory *Y*-axis is defined as an axis perpendicular to the plane of polarization of the X-ray *e* vector and is the same axis as the rotation axis ϕ. The laboratory *Z*-axis is defined as the direction of propagation of the X-rays.

XANES and EXAFS spectra were recorded at room temperature on beamline 9-3 at SSRL (Stanford Synchrotron Radiation Laboratory) and beamline 10.3.2 at ALS (Advanced Light Sources). At SSRL BL 9-3, the synchrotron ring SPEAR was operated at 3.0 GeV at 50−100 mA beam current. Energy resolution of the focused incoming X-rays was achieved using a Si(220) double-crystal monochromator, which was detuned to 50% of maximal flux to attenuate second harmonic X-rays. A N_2-filled ion chamber (I_0) was mounted in front of the sample to monitor incident beam intensity. An incident X-ray beam of 1 mm (horizontal) × 1 mm (vertical) dimension was used for the XANES and EXAFS experiments. The single-crystal X-ray absorption spectra were collected as fluorescence excitation spectra using a 30-element energy-resolving detector from Canberra Electronics. The isotropic powder spectra were collected in a similar manner, except that a non-energy-resolving ionization chamber (Lytle detector) was used for detection. At ALS BL 10.3.2,[47] the synchrotron ring was operated at 1.9 GeV at 200−400 mA beam current. Energy resolution of the focused incoming X-rays was achieved using a Si(111) double-crystal monochromator. Spectra were collected in fluorescence with a 7-element Ge detector and in transmission with an ionization chamber. An incident X-ray beam of 0.1 mm (horizontal) × 0.02 mm (vertical) dimension was used for the XANES and EXAFS experiments. This spot size is large compared to what the beamline normally produces and was obtained by moving the sample downstream of focus. The beam was defocused in order to reduce radiation damage to the sample. Combined XANES/EXAFS spectra were collected, and the details are described in the Supporting Information. Data reduction for the XANES and EXAFS spectra was performed as described previously.[48]

Curve fitting of the EXAFS spectra from single crystals was carried out using previously described procedures[48] to isolate all of the Fourier peaks together ($\Delta R' \sim 1.2-5$ Å). These isolates were then fit using ab initio-calculated phases and amplitudes from the program FEFF 8 from the University of Washington.[49] The ab initio phases and amplitudes were calculated from the crystallographic data.[30,32]

(43) DeBeer George, S.; Brant, P.; Solomon, E. I. *J. Am. Chem. Soc.* **2005**, *127*, 667−674.
(44) Scott, R. A.; Hahn, J. E.; Doniach, S.; Freeman, H. C.; Hodgson, K. O. *J. Am. Chem. Soc.* **1982**, *104*, 5364−5369.
(45) Flank, A. M.; Weininger, M.; Mortenson, L. E.; Cramer, S. P. *J. Am. Chem. Soc.* **1986**, *108*, 1049−1055.
(46) Workman, J. M.; Powell, R. D.; Procyk, A. D.; Collins, T. J.; Bocian, D. F. *Inorg. Chem.* **1992**, *31*, 1548−1550.
(47) Marcus, A. M. Description of Beamline 10.3.2., http://xraysweb.lbl.gov/uxas/Index.htm.
(48) Robblee, J. H.; Messinger, J.; Cinco, R. M.; McFarlane, K. L.; Fernandez, C.; Pizarro, S. A.; Sauer, K.; Yachandra, V. K. *J. Am. Chem. Soc.* **2002**, *124*, 7459−7471.
(49) Rehr, J. J.; Albers, R. C. *Rev. Mod. Phys.* **2000**, *72*, 621−654.

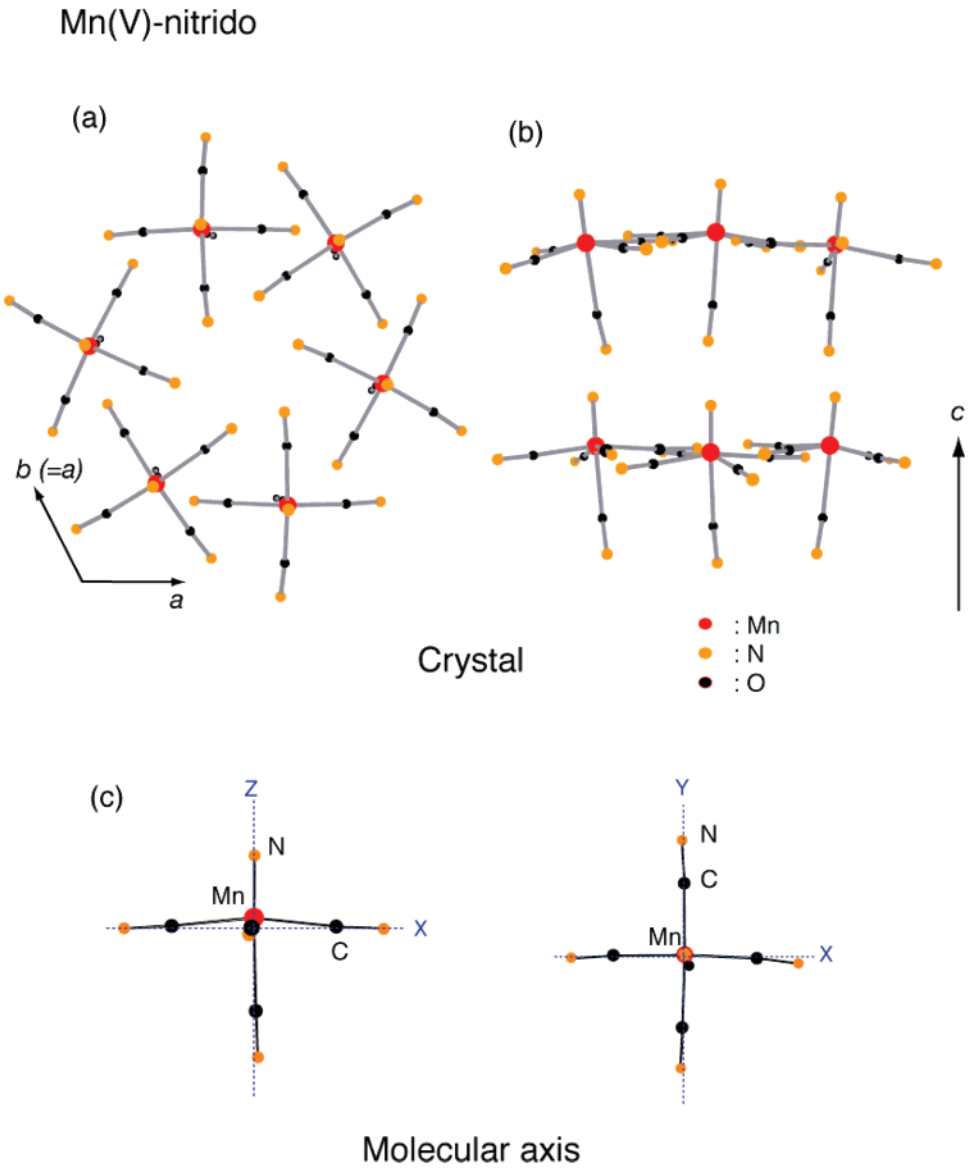

Figure 1. Crystal and molecular structures of Mn(V)-nitrido compound. (a and b) Molecular arrangement in the crystal unit cell and (c) molecular structure. The molecular *z*-axis (Mn≡N direction) is aligned nearly parallel to the crystal *c*-axis (9.4° off). The Mn position is ~0.2 Å displaced out of the equatorial ligand plane toward the nitrido ligand.

Pre-edge fits were performed using EDG_FIT.[50] After background subtraction, pre-edge components were fit with pseudo-Voigt functions.

X-ray Diffraction Measurement. For each polarized XAS measurement, XRD was taken in situ by placing the X-ray diffraction detector downstream of the sample in order to obtain the relationship of the crystal axes and the *e* vector of the incident X-ray beam. Diffraction data were collected using a Mar 345 imaging plate (BL 9-3) or Bruker SMART 2000 CCD (BL 10.3.2) in single shot mode with a 60 s exposure. Diffraction spots were indexed with Mosflm,[51] using the known unit cell parameters.[30,32] The published atomic coordinates were used to determine the orientation of specific molecular directions relative to the crystal axes.

Polarized X-ray Absorption Spectroscopy. XANES spectra mainly reflect electric-dipole-allowed transitions from the initial state. However, weak pre-edge features are observed for transition metals in a centrosymmetric environment which are due to electric-quadrupole-allowed 1s to 3d transitions.[37,39,52] When the inversion symmetry is eliminated, however, the pre-edge transitions can gain intensity through the metal 4p orbital character mixing into the metal 3d orbitals. It is estimated that electric dipole transitions are 2 orders of magnitude more intense than electric quadrupole transitions.[42] Thus only a few percent 4p mixing into the 3d orbitals can yield significant pre-edge intensity.

The intensity of the polarized XAS spectra, governed primarily by electric dipole mechanism, is related to the density of final states (*f*) of the appropriate symmetry which has a measurable overlap with the initial state wavefunction (*i*). The X-ray absorption cross section for the electric-dipole-allowed transition, σ_D, is given by the equation

$$\sigma_D \propto |\sum_j e_j \langle f|r_j|i\rangle|^2 \qquad (1)$$

where e_j and r_j ($j = x, y, z$) are the direction cosines of the X-ray *e* vector and the transition moment operator. The cross section is proportional to the sum of all contributing molecular orientations in

(50) George, G. N. *EXAFSPAK and EDG_FIT*; Stanford Synchrotron Radiation Laboratory, Stanford Linear Accelerator Center, Stanford University: Stanford, CA 94309, 2000.
(51) Leslie, A. G. W.; Powell, H. *Mosflm*, 6.2.3; Cambridge.
(52) Brouder, C. *J. Phys.: Condens. Matter* **1990**, *2*, 701−738.

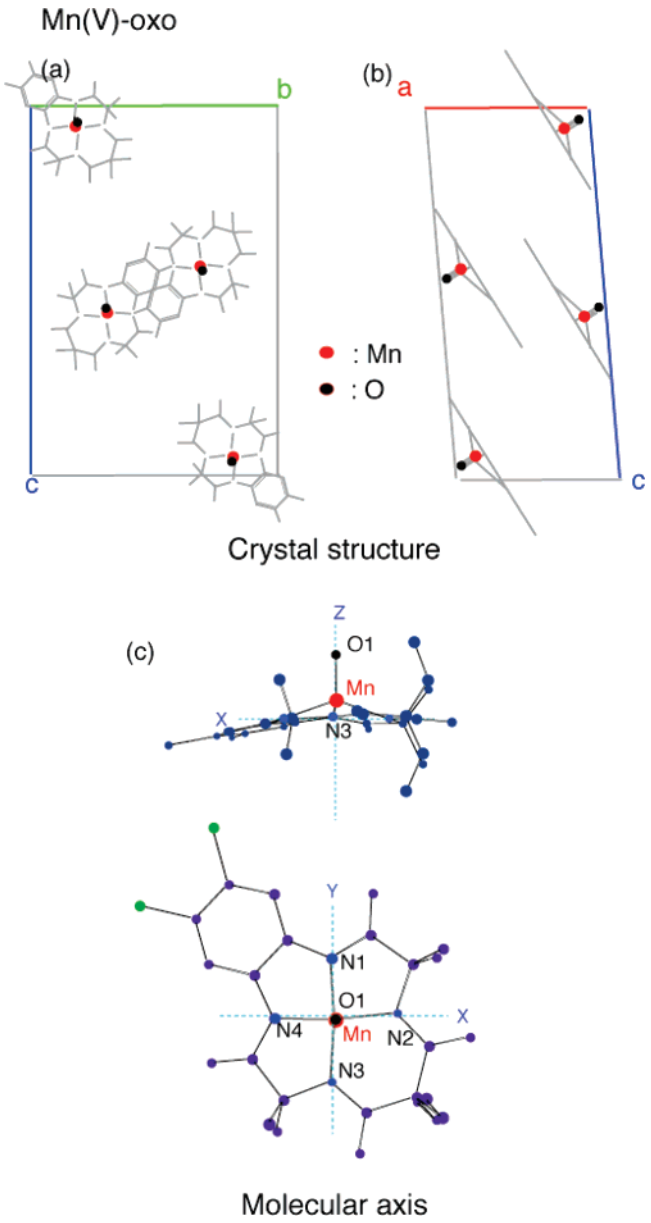

Figure 2. Crystal and molecular structures of Mn(V)-oxo compound. (a and b) Molecular arrangement of DCB in the crystal and (c) molecular structure of DCB. The molecular *z*-axis (Mn≡O direction) is tilted about 60° from the crystal *c*-axis. The macrocyclic planes are oriented almost parallel to each other (b), but rotated to each other about 90° (a). The Mn position is ~0.6 Å displaced out of the equatorial ligand plane toward the nitrido ligand.

the crystal, and the amplitude of each pre-edge component is weighted by $\cos^2\theta$, where θ is the angle between the X-ray *e* vector and the molecular transition dipole vector. Therefore, when an oriented crystal is aligned with a known molecular orientation, the angular dependence of the intensity of a particular absorption feature may be used to determine the symmetry of the final state wavefunction.

For pre-edge features which only gain intensity through electric-quadrupole-allowed transitions, the absorption cross section (σ_Q) can be rewritten as

$$\sigma_Q \propto |\sum_j \sum_n e_j k_n \langle f|r_j r_n|i\rangle|^2 \qquad (2)$$

where k_n and e_j are the direction cosines of the X-ray propagation direction and the X-ray *e* vector and r_n and r_j are the transition moment operators. Now the dichroism is the result of the combination of the orientations of e_j and k_n vectors.

Equations 1 and 2 describe the pure dipole and quadrupole contribution. However, the absorption cross section is a sum of eqs 1 and 2, which is determined by the chemical and geometric structure around the metal.

Specific edge or pre-edge features which are unresolved in solution XAS can be orientationally selected and resolved in polarized XAS. One can also discriminate between dipole and quadrupole transitions based on their polarization behavior.

Electronic Structure Calculations. All calculations in this study were performed with the electronic structure program ORCA.[53] Single-point spin-unrestricted density functional calculations using the crystallographic coordinates were carried out with the BP86 functional.[54−58] All electron-polarized triple-ξ (TZVP) Gaussian basis sets of the Alrichs group were used for all atoms.[59] Calculated XAS spectra were obtained by performing time-dependent density functional theory (TD-DFT) calculations, allowing for excitation of the Mn 1s electrons.[60,61]

Results

I. Polarized XAS Spectroscopy. A. Mn(V)≡nitrido Spectra. The XANES and EXAFS spectra of the Mn(V)-nitrido single crystals and the XANES spectrum of a powder sample are shown in Figure 3. The crystal has a pencil-like morphology, in which the 6-fold axis coincides with the crystallographic *c*-axis. The polarized spectra were taken by changing the χ-angle as shown in Figure 3a (top right). The crystal *c*-axis is parallel to the X-ray *e* vector at the $\chi = 0°$ orientation and perpendicular to it at the $\chi = 90°$ orientation. The intense pre-edge feature at 6542.9 eV in Figure 3a has pronounced dichroism with maximum intensity when the crystal *c*-axis is parallel to the X-ray *e* vector ($\chi = 0°$) and minimum intensity when the *c*-axis is perpendicular to the *e* vector ($\chi = 90°$). The crystal *c*-axis in this system almost coincides with the Mn≡N bond direction (the molecular *z*-axis, see Figure 1c), suggesting that the strong pre-edge transition mainly occurs along the molecular *z* direction. This is also confirmed by the polarization characteristics of EXAFS in Figure 3b (for *k*-space data, see Supporting Information). The intense peak at an apparent distance R' of 1.18 Å in the $\chi = 0°$ spectrum is due to backscattering from the axial nitrido atom, while the peak at R' of 1.53 Å in the $\chi = 90°$ spectrum is due to backscattering from the four equatorial C atoms. The peak at $R' = 2.58$ Å arises from the N atoms in the equatorially bound cyano groups and is strongly enhanced by multiple scattering mediated by the intervening collinear C atoms (for the detailed curve fitting results, see Supporting Information).

Figure 3a (top) shows the XANES spectra of an isotropic powder sample. The pre-edge peak is much less intense (~39% of the intensity) than the polarized spectrum collected at $\chi = 0°$, which provides the maximum projection of the X-ray *e*

(53) Neese, F. *ORCA-an ab initio, DFT, and Semiempirical Electronic Structure Package*, version 2.6; University of Bonn: Bonn, Germany, 2003.
(54) Geometry-optimized calculations were also performed; however, it was found that the axial Mn−CN bond trans to the nitrido was ~0.1 Å longer than in the experimental structure. This is consistent with previously reported calculations (refs 55 and 56).
(55) Hummel, P.; Gray, H. B. *Coord. Chem. Rev.* **2007**, *251*, 554−556.
(56) Bendix, J.; Meyer, K.; Weyhermuller, T.; Bill, E.; Metzler-Nolte, N.; Wieghardt, K. *Inorg. Chem.* **1998**, *37*, 1767−1775.
(57) Becke, A. D. *J. Chem. Phys.* **1986**, *84*, 4524−4529.
(58) Perdew, J. P.; Yue, W. *Phys. Rev. B* **1986**, *33*, 8800−8802.
(59) Schafer, A.; Horn, H.; Ahlrichs, R. *J. Chem. Phys.* **1992**, *97*, 2571−2577.
(60) Ray, K.; DeBeer George, S.; Solomon, E. I.; Wieghardt, K.; Neese, F. *Chem.—Eur. J.* **2007**, *13*, 2783−2797.
(61) DeBeer George, S.; Petrenko, T.; Neese, F. *Inorg. Chim. Acta*, in press.

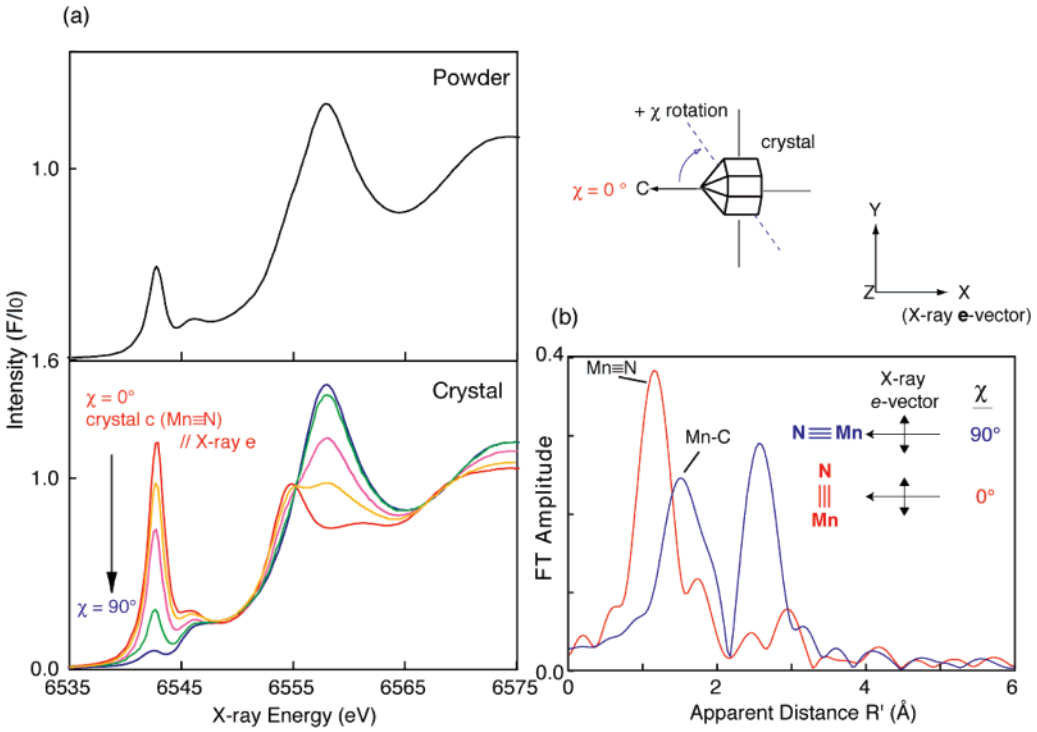

Figure 3. Polarized Mn XANES (a) and Fourier transformed EXAFS (k^3-weighted) spectra (b) of Mn(V)-nitrido compound. For a comparison, XANES spectrum of the powder sample is shown in (a), top. The crystal was at first set such that the crystal *c*-axis is parallel to the X-ray *e* vector ($\chi = 0°$ orientation, see top right), which is parallel to the laboratory *X*-axis. Polarized spectra were taken at various χ orientations ($\chi = 0$, 30, 45, 70, and 90°). The arrow shows the direction that the spectral features change as χ is increased from 0 to 90°, thereby decreasing the overlap between the Mn≡N bond and the X-ray *e* vector. For EXAFS, only the spectra from two extreme orientations ($\chi = 0$ and 90°) are shown.

vector on the Mn≡N bond. This is expected, because the isotropic sample contains a distribution of Mn≡N bonds in all possible orientations. The amplitude of the polarized features is weighted by $\cos^2\theta$, where θ is the angle between the Mn− backscatterer vector and the X-ray *e* vector. Thus, the $\cos^2\theta$ term must be averaged over all orientations in the sphere, which produces a weighting factor of 1/3. To properly compare the oriented single-crystal data with the data from isotropic samples, it is therefore necessary to divide the oriented data by $3\cos^2\theta$. A close examination of the crystal structure of this system shows that the molecular *z*-axes of the four molecules/unit cell are equally displaced from the crystallographic *c*-axis by ±9.4°. By taking this molecular alignment into account, the calculated intensity of the powder spectrum is 34.2% of the $\chi = 0°$ polarized pre-edge peak. The slightly higher experimental value (~39 ± 1%) may suggest that there are some other transition components which contribute in this energy range.

The pre-edge spectra of single crystal ($\chi = 0-90°$) and powder samples were fit with pseudo-Voigt functions (Table 1). The peak position at 6542.9 eV is constant through $\chi = 0-70°$ regardless of the crystal orientation, suggesting the presence of a single predominant 1s → 3d transition. The nonzero amplitude of the pre-edge features at the Mn≡N ⊥ X-ray *e* vector ($\chi = 90°$) could be due to contributions from the other 1s → 3d transitions and the fact that a 9.4° angle exists between the Mn≡N vectors and the crystallographic *c*-axis.[62] This nonalignment of the molecules accounts for ~3% of the residual intensity in the pre-edge feature at $\chi = 90°$, which is in good agreement with the experimental value (3.1% residual

Table 1. Pre-edge Fitting of the Mn(V)-nitrido Complex[a]

χ (deg)	peak (eV)	amp	HWHM (eV)	area
0	6542.9	0.97	**0.81**	1.98
30	6542.9	0.80	**0.81**	1.63
45	6542.9	0.57	**0.81**	1.16
70	6542.9	0.21	**0.81**	0.42
90	6542.6	0.03	**0.81**	0.06
powder	6542.9	0.39	**0.81**	0.79

[a] Bold numbers indicate the fixed values. The Gaussian/Lorentzian fraction parameter was fixed to 0.5.

in intensity). However, we observe a 0.3 eV of peak shift[63] at the 90° orientation, which may suggest the presence of a low-energy transition polarized in the equatorial ligand plane.

There is an additional peak above the pre-edge but below the rising edge at 6545.7 eV observed in all crystal orientations. The nondichroic nature of this peak suggests that this transition is mediated by the cyanide group.

The main edge region, which contains the 1s → 4p transition (approximately 6545−6580 eV), is also significantly dichroic, showing at least two distinguishable components; the lower component shows the same polarization characteristic as the pre-edge peak (polarized parallel to the molecular *z*-axis), while the higher one shows the opposite dichroism. The higher component is presumably from multiple-scattering contributions from the five cyanide ligands to the Mn atom. Although interpretation of the main edge region is beyond the scope of the present study, this type of behavior has been seen in other compounds with strong multiple-scattering paths.[40]

(62) Additional effect arises from the imperfect polarization (~95%) of the beam.

(63) The experimental energy resolution is <0.2 eV.

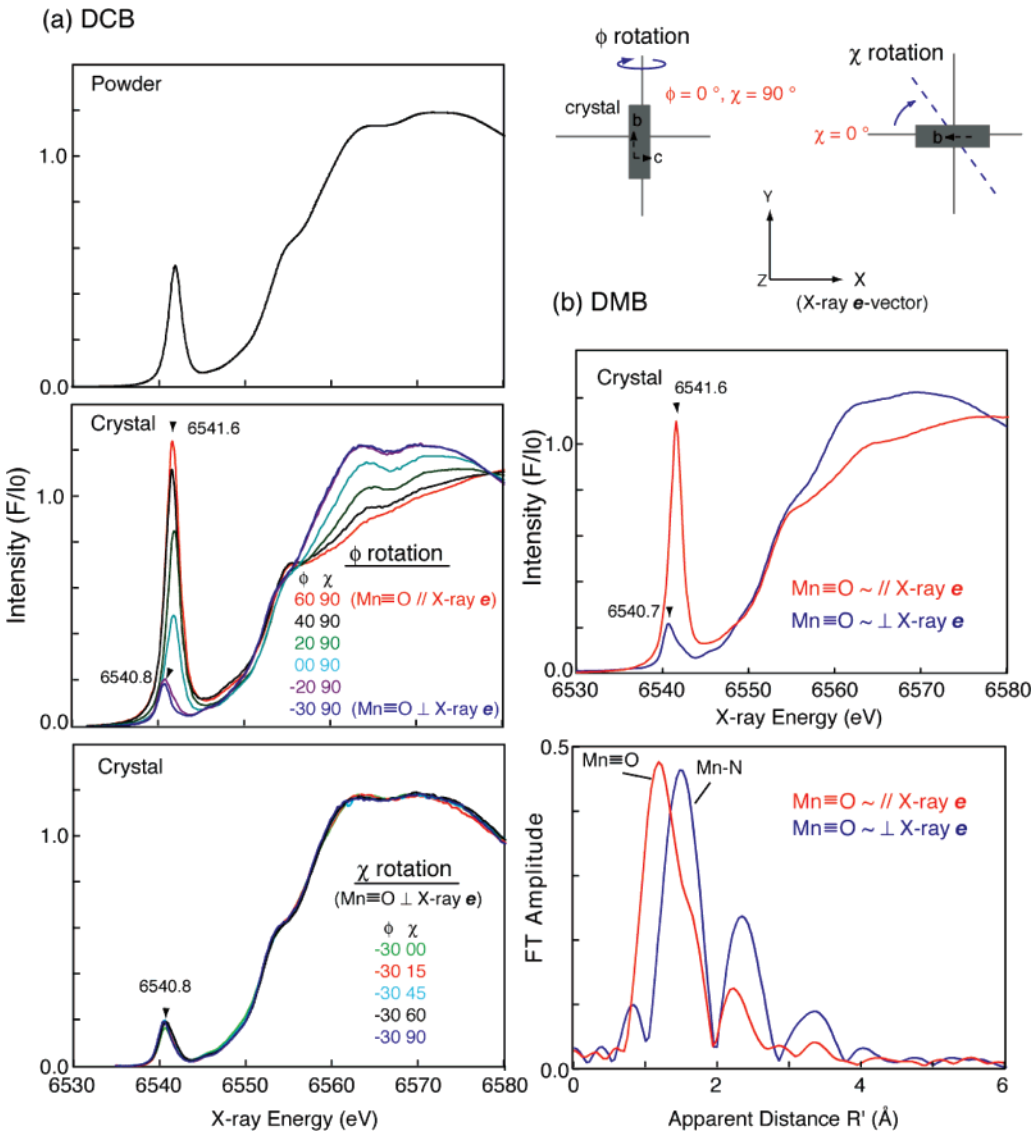

Figure 4. Polarized Mn XAS spectra of Mn(V)-oxo compounds, (a) DCB and (b) DMB. For DMB and DCB, the crystal was at first set such that the long axis of the crystal is parallel to the laboratory *Y*-axis ($\chi = 0°$, $\phi = 90°$ orientation), and polarized spectra were taken by rotating the crystal around the laboratory *Z*- (χ rotation) and *Y*-axes (ϕ rotation). (a) The middle figure shows the polarized spectra out of the macrocyclic ligand plane (ϕ varied, $\chi = 90°$) and the bottom figure in the macrocyclic plane ($\phi = -30°$, χ varied). (b) Polarized XAS spectra of DMB in the two extreme orientations, XANES (middle) and EXAFS (bottom).

B. Mn(V)-oxo Spectra. Figure 4 shows the XANES and EXAFS spectra of the Mn(V)-oxo compounds. In this system, the crystals are needle-shaped and the molecular axes are not co-incident with any of the crystallographic axes (Figure 2). The crystal was at first oriented such that the needle long axis is nearly parallel to the X-ray *e* vector, and this orientation was defined as $\phi = 0°$, $\chi = 90°$. Polarized spectra were collected at various ϕ and χ orientations using the Mn(V)-oxo(DCB) compound (Figure 4a) since the crystal structure has been reported only for this compound. The precise crystal orientation was determined from the X-ray diffraction pattern taken at each orientation within an accuracy of $\pm 2°$. The polarized spectra collected as a function of χ and ϕ rotations (Figure 4, middle and bottom) show the dichroism out of the macrocyclic ligand plane (ϕ varied, $\chi = 90°$) and within the macrocyclic plane ($\phi = -30°$, χ varied). For the Mn(V)-oxo(DMB) compound, polarized spectra at only two extreme orientations are shown with the corresponding EXAFS spectra (Figure 4b). Overall spectral shape and polarization characteristics were almost identical for the two Mn(V)-oxo compounds, suggesting isomorphic crystal structures.

A strongly dichroic pre-edge feature similar to the Mn(V)-nitrido compound is observed in the Mn(V)-oxo compounds. Unlike the Mn(V)-nitrido compound, the pre-edge peak energy position of the Mn-oxo compound changes depending on the crystal orientation, indicating that there are two contributions to this region. These two components have different polarization characteristics. The high-energy peak at 6541.6 eV is significantly enhanced at the $\phi = 60°$, $\chi = 90°$ orientation when the X-ray *e* vector is parallel to the Mn≡O bond. The presence of the low-energy component (6540.8 eV), which was not observed in the powder spectrum, became visible in the polarized spectra at the $\phi = -30°$ orientation due to the negligible contribution of the strong high-energy component. This peak is the only observable component when the crystal is rotated within the plane of the macrocyclic ligand (χ rotation, Figure 4a, bottom). The relation between the pre-edge dichroism and the molecular orientation is also clear from the XANES and EXAFS of Mn-

Table 2. Pre-edge Fitting of the Mn(V)-oxo(DCB) Complex[a]

ϕ (deg)	χ (deg)	peak (eV)	amp	HWHM (eV)	area	peak (eV)	amp	HWHM (eV)	area
60	90	**6540.8**	0.12	**0.95**	0.24	**6541.6**	1.17	**0.8**	2.77
50	90	**6540.8**	0.12	**0.95**	0.24	**6541.6**	1.15	**0.8**	2.72
40	90	**6540.8**	0.13	**0.95**	0.26	**6541.6**	1.05	**0.8**	2.48
30	90	**6540.8**	0.09	**0.95**	0.18	**6541.6**	0.95	**0.8**	2.25
20	90	**6540.8**	0.05	**0.95**	0.11	**6541.6**	0.80	**0.8**	1.89
10	90	**6540.8**	0.03	**0.95**	0.06	**6541.6**	0.70	**0.8**	1.66
0	90	**6540.8**	0.06	**0.95**	0.12	**6541.6**	0.44	**0.8**	1.04
−10	90	**6540.8**	0.18	**0.95**	0.36	**6541.6**	0.17	**0.8**	0.40
−20	90	**6540.8**	0.17	**0.95**	0.34	**6541.6**	0.07	**0.8**	0.17
−30	90	**6540.8**	0.17	**0.95**	0.34	**6541.6**	0.02	**0.8**	0.05
powder		**6540.8**	0.14	**0.95**	0.28	**6541.6**	0.35	**0.8**	0.82

[a] Bold numbers indicate the fixed values. The Gaussian/Lorentzian fraction parameter was fixed to 0.5.

(V)-oxo(DMB). The pre-edge peak at 6541.6 eV becomes most intense when the shortest FT peak ($R' = 1.2$ Å in Figure 4b, bottom, which corresponds to the Mn≡O interaction) becomes most intense. The lower-energy component becomes dominant when the EXAFS peak at R' of 1.5 Å becomes intense. This peak corresponds to the backscattering from the equatorial N ligands in the macrocycle. The details of the EXAFS fitting result are in the Supporting Information.

Table 2 shows the curve fitting result of the pre-edge peaks of Mn(V)-oxo (DCB) during ϕ rotation (the spectra in Figure 4a, middle). This ϕ angular dependence of the pre-edge components (6541.6 and 6540.8 eV) is plotted in Figure 5 together with the result of Mn(V)-nitrido compound (χ angular dependence of 6542.9 eV component shown in Figure 3a and Table 1). The intensity of the peak at 6541.6 eV (6542.9 eV for Mn(V)-nitrido) changes according to the $\cos^2\theta$ relation between the Mn≡O vector (or Mn≡N for Mn(V)-nitrido) and X-ray e vector (black dotted lines in Figure 5). On the other hand, the dichroism of the peak at 6540.8 eV of the Mn(V)-oxo compound seems to have a more complicated orientation dependence that does not show a simple $\cos^2\theta$ dependence with the X-ray e vector. This could be due to a significant quadrupole contribution, which depends on the X-ray propagation direction (k vector) in addition to the dependence on the X-ray e vector (see eq 2). In fact, the intensity of the 6540.8 eV peak is best fit with the combination of the dipole (σ_D) and quadrupole (σ_Q) character (see Supporting Information). However, the error (±0.07 units in amplitude) which is attributed to both the misalignment of crystal and curve fitting is considerably larger, and thus further discussion of the contribution of dipole versus quadrupole contributions to the experimental data is not warranted. This peak does not show noticeable dichroism when the crystal is rotated within the plane of the macrocyclic ligand (Figure 4a, bottom). This is attributed to the molecular arrangement in the unit cell, as the neighboring molecules are rotated about 90° from each other.

The dichroism in the main edge region is much less dramatic than that seen in Figure 3 for the Mn(V)-nitrido single crystal, in part because multiple-scattering contributions are much smaller for the five-coordinate Mn(V)-oxo complex (see Figure 1). Additionally, the Mn is displaced from the equatorial ligand plane by ~0.6 Å in the Mn(V)-oxo compounds, compared to ~0.2 Å in the Mn(V)-nitrido compound. Multiple-scattering effects are strongly dependent on the collinearity of the absorber, backscatterer, and intervening atom.

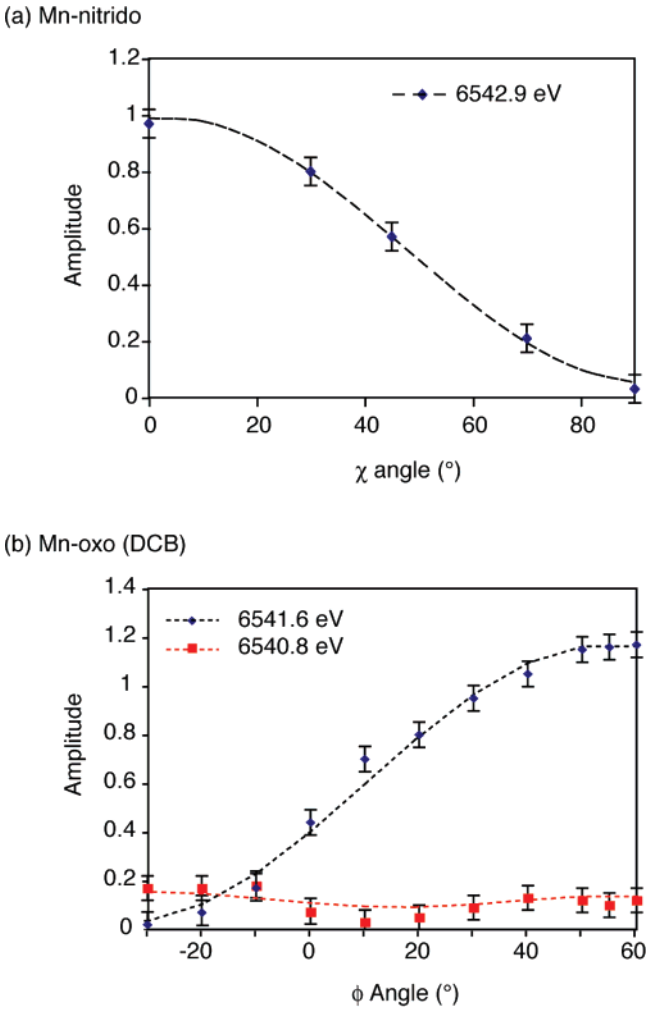

Figure 5. Angular dependence of the pre-edge peaks of (a) Mn(V)-nitrido and (b) Mn(V)-oxo(DCB) complexes. The pre-edge amplitude values for the Mn(V)-nitrido (Table 1) and the Mn(V)-oxo(DCB) (Table 2) were plotted; in (a) Mn(V)-nitrido complex, the black points show the intensity of the 6542.9 eV peak, and in (b) Mn(V)-oxo (DCB) complex, the black and red points are of the 6541.6 and 6540.8 eV peaks. For the 6542.9 eV (a) and 6541.6 eV (b) components, the black dotted lines are the fit of the intensity to the $A\sigma_D + B$ function, which show a simple $\cos^2\theta$ dependence ($\sigma_D \propto \cos^2\theta$). On the other hand, the 6540.8 eV component was best fit with a combination of quadrupole and dipole character, $A\sigma_D + B\sigma_Q + C$, where A, B, and C are constants (see Supporting Information). The definition of the χ or ϕ angle of each compound is described in Figure 3 (for Mn(V)-nitrido) and Figure 4 (for Mn(V)-oxo), respectively. The error bars are mainly due to the crystal misalignment and the curve fitting results.

II. Electronic Structure Calculations. Ground-state DFT calculations have been used to obtain electronic structure descriptions of the Mn(V)-nitrido and Mn(V)-oxo complexes. The orbital compositions for the metal-based d orbitals are summarized in Table 3, and the spin-down metal-based molecular orbitals are shown in Figure 6.

For the Mn(V)-nitrido compound, the d_{xy} orbital is the HOMO (MO 49) and is dominated by π-interactions with the cyanide ligands. The d_{xz} and d_{yz} orbitals form doubly degenerate LUMOs (MOs 50, 51), with significant π-interactions with the axial nitrido and smaller contributions from the cyanides. The $d_{x^2-y^2}$ orbital (MO 52) comprises primarily σ-bonding interactions with the cyanides. At the highest energy is the d_{z^2} orbital (MO 53), which has significant contributions from σ-interactions with both the nitrido and the cyanides, as well as a significant (6.5%) Mn

Table 3. Results of Calculations for the Five Metal d-Based Orbitals in the Mn(V)-nitrido and Mn(V)-oxo Complexes

			Mn(V)-nitrido			
MO label	49 (d_{xy})	50 (d_{xz})	51 (d_{yz})	52 ($d_{x^2-y^2}$)	53 (d_{z^2})	total
energy (eV)	−4.56	−2.09	−2.09	−0.70	−0.16	
			orb contribution:			
Mn 3d total	74.0	45.3	45.1	58.4	25.2	248.0
Mn $4p_x$	0	0.3	0	0	0	
Mn $4p_y$	0	0	0.3	0	0.1	
Mn $4p_z$	0	0	0	0	6.5	
Mn 4p total	0	0.3	0.3	0.0	6.6	7.2
nitrido	0.2	43.5	43.4	0	14.5	101.6
cyanides	25.3	10.5	10.5	40.8	51.0	138.1
			Mn(V)-oxo			
MO label	137 (d_{xy})	139 (d_{xz})	140 (d_{yz})	141 (d_{z^2})	142 ($d_{x^2-y^2}$)	total
energy (eV)	−5.47	−3.9	−3.7	−3.1	−2.74	
			orb contribution:			
Mn 3d total	72.1	57.1	57.2	44.8	53.2	284.4
Mn $4p_x$	0	0.5	0.1	0	0.5	
Mn $4p_y$	0.1	0	0.4	0.3	0	
Mn $4p_z$	0	0	0.1	5.4	0	
Mn 4p total	0.1	0.5	0.6	5.7	0.5	7.4
oxo	0.9	16.6	20.4	22.3	21.8	82.0
macrocycle	23.7	23.5	19.3	25.2	36.0	127.7

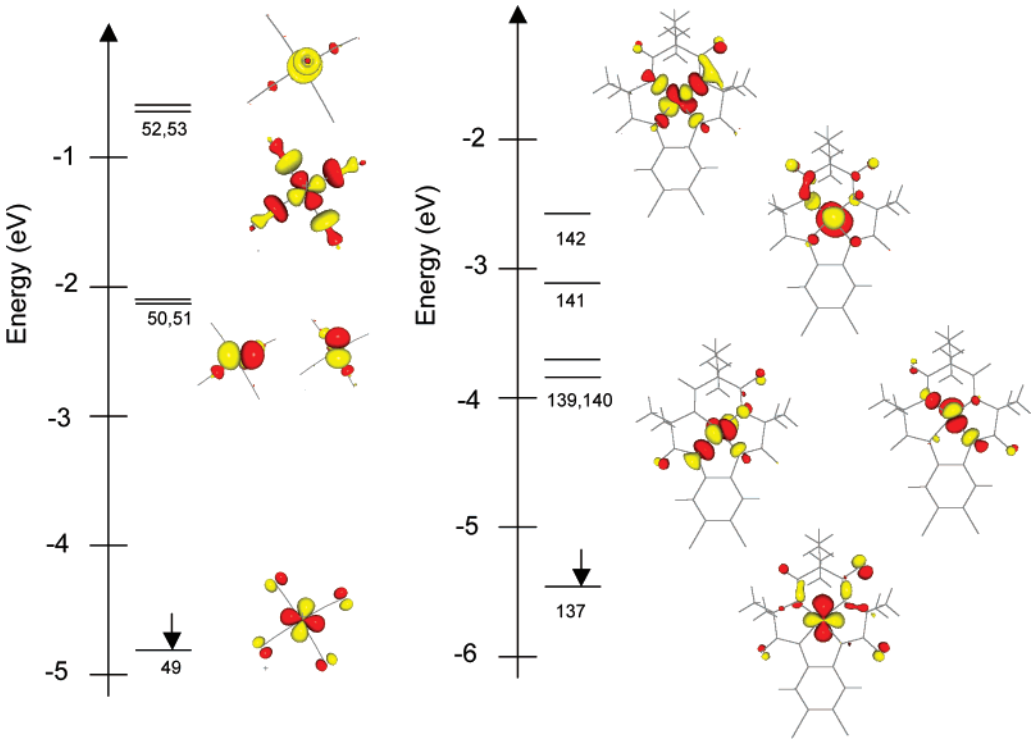

Figure 6. Spin-down molecular orbitals for the Mn(V)-nitrido (left) and Mn(V)-oxo (right) complexes.

$4p_z$ contribution. The general electronic structure description is consistent with that previously reported by Bendix et al.[32] and more recently by Hummel and Gray.[55]

For the Mn(V)-oxo compound, the d_{xy} orbital (MO 137) is the HOMO, with significant contributions from the DCB macrocycle. The LUMO (MO 138) is a primarily ligand-based orbital with no significant metal contribution and therefore not shown here. The d_{xz} and d_{yz} orbitals (MOs 139, 140) are doubly degenerate set, with contributions from π-type interactions with the axial oxo ligand and a small but significant (1.0% total) Mn $4p_{x,y}$ contribution. The d_{z^2} orbital (141) has a large contribution from a σ-interaction with the axial oxo (22.3%) and significant (5.4%) $4p_z$ mixing. At the highest energy is the $d_{x^2-y^2}$ orbital (142) which has significant contributions from both a π-type interaction with the axial oxo and σ-interactions with the DCB macrocycle.

As discussed above, the pre-edge region of a Mn *K*-edge spectrum results from weak quadrupole-allowed 1s to 3d transitions, which primarily gain intensity through the mixing of metal 4p character into these orbitals giving the transitions significant electric dipole character. Hence, for the Mn(V)-nitrido, the calculations indicate a significant pre-edge feature due to the 1s to $3d_{z^2}$ (+6.5% $4p_z$) transition, with no significant contributions from the remaining d orbitals. In the case of the Mn(V)-oxo, the calculations indicate that transitions to both the doubly degenerate d_{xz},d_{yz} orbitals (+1.0% $4p_{x,y}$) and the d_{z^2}

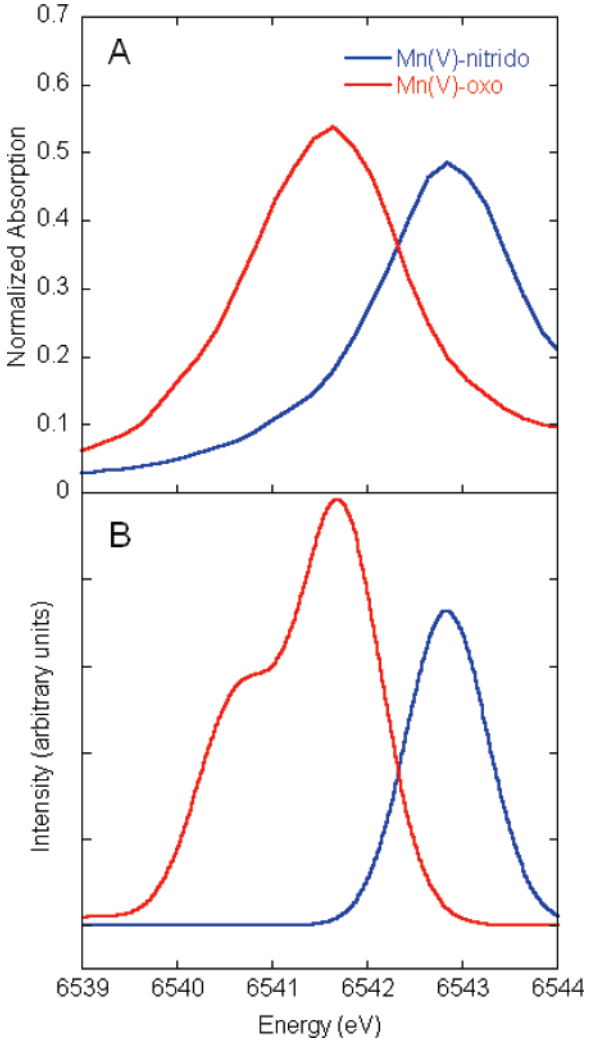

Figure 7. Comparison of the experimental isotropic (A) and TD-DFT calculated (B) Mn *K*-pre-edge XAS spectra of the Mn(V)-nitrido and the Mn(V)-oxo complexes. A 1 eV broadening was used for the calculated spectra. A constant shift of 168.2 eV has been applied to all calculated spectra.

orbital (+5.4% $4p_z$) will give rise to significant dipole-allowed intensity. This should result in a weaker (d_{xz},d_{yz}) pre-edge peak ~0.7 eV below a more intense (d_{z^2}) pre-edge peak.

In order to more clearly illustrate the trends shown by the ground-state DFT calculations, we have carried out TD-DFT calculations allowing for excitation of only the Mn 1s electrons. Figure 7 shows a comparison of the isotropic experimental data (panel A) to the calculated pre-edges (panel B) of the Mn(V)-nitrido and Mn(V)-oxo complexes.[64] In both cases, the pre-edge intensities can be understood based dominantly on electric-dipole-allowed transitions. Weak quadrupole transitions are also expected but have not been calculated. The calculated Mn(V)-nitrido spectrum is dominated by a single intense pre-edge peak which is due to 6.5% $4p_z$ mixing into the $3d_{z^2}$ molecular orbital, as discussed above. This mixing is mediated by the deviation from inversion symmetry caused by the short Mn−N(nitrido) bond. No other transitions with significant intensity are calculated for the Mn(V)-nitrido complex in the pre-edge region.[65]

The calculated Mn(V)-oxo complex also has an intense pre-edge feature (due to 5.4% $4p_z-3d_{z^2}$ mixing). However, a weaker feature to 0.7 eV lower energy is also present, which is due to 1.0% $4p_{xy}$ mixing into the d_{xz}/d_{yz} molecular orbitals. This may be attributed to the greater displacement of the Mn from the plane of the Mn(V)-oxo macrocycle. For Mn(V)-nitrido compound, the Mn and the four equatorial carbons are nearly in the plane, with a displacement of only ~0.2 Å. However, for the Mn(V)-oxo compound, the Mn is displaced by ~0.6 Å from the equatorial plane. This distortion from the *xy*-plane allows for $4p_{x,y}$ mixing into the $3d_{xz,yz}$, giving this transition dipole-allowed character.

The calculated spectra generally show very good agreement with experiment. The calculated energy difference between the Mn(V)-nitrido and Mn(V)-oxo pre-edge energy maxima is 1.1 eV, as compared to an experimental separation of 1.3 eV. The higher pre-edge energy for the Mn(V)-nitrido complex reflects both the presence of a sixth ligand and the larger σ-donation from the multiple donor (nitrido and cyanides), which raises the energy of the d_{z^2} relative to the five-coordinate oxo complex. The calculated intensity ratio for the Mn(V)-nitrido to Mn(V)-oxo pre-edge intensity is 1:2, in reasonable agreement with the experimentally observed intensity ratio of 1:1.4 (Table 2). The relative splittings of the two Mn(V)-oxo pre-edge features are also well-reproduced by the calculation, giving an energy splitting of 0.7 eV (vs the experimental 0.8 eV splitting). However, the relative calculated intensity ratio for the lower energy to the higher energy peak is slightly overestimated, with a calculated ratio of 0.54:1.0 (vs the experimental 0.34:1.0 intensity ratio (Table 2)).

Discussion

Polarized X-ray absorption spectroscopy on single crystals significantly expands the electronic structural information over what is gleaned from studies of isotropic samples. Using the Mn(V) systems, we have demonstrated the advantage of this methodology combined with DFT calculations. The X-ray diffraction patterns taken in situ are used to align crystals in a certain orientation based on the known crystal structure. Polarized spectra allow us to orientationally resolve peak components, and each component can be analyzed and interpreted by the relation between the molecular orientation and polarization characteristics. Polarized EXAFS spectra provide further support of the relation between the molecular orientation and the electronic transition.

Comparison of pre-edge and EXAFS spectra of the Mn(V) compounds clearly shows that the strong pre-edge peak is due to the transition component along the Mn(V)≡N or Mn(V)≡O bonds. Additionally, for the Mn(V)-oxo compound, an unresolved low-energy component in the powder spectrum becomes visible when the polarized spectra are taken along the macrocyclic plane. Using polarized Mn *K*-edge XAS data coupled to electronic structural calculations, we are able to understand the origins of the Mn(V)-nitrido and Mn(V)-oxo pre-edge features.

In general, the pre-edge region of a Mn *K*-edge spectrum results from weak quadrupole-allowed 1s to 3d transitions, which primarily gain intensity through the mixing of metal 4p character

(64) Due to shortcomings of the DFT potentials in the core regions, a constant shift of 168.2 eV has been applied to all calculated spectra.

(65) It should be noted that the 0.6% total intensity in the d_{xz} and d_{yz} orbitals does not yield significant transition intensity as the calculated oscillator strength for these transitions is an order of magnitude smaller.

into these orbitals giving the transition significant electric dipole character. The intensity of electric quadrupole-allowed transitions is generally ~1% of electric-dipole-allowed transitions,[66] indicating that a small amount of metal 4p mixing into the metal 3d orbital will dominate the pre-edge intensity. For both the Mn(V)-nitrido and the Mn(V)-oxo complexes, the short axial nitrido/oxo distances (1.57 Å for Mn(V)-nitrido and 1.55 Å for Mn(V)-oxo) induce a strong ligand field distortion of the metal site from octahedral environment, resulting in symmetry-allowed 3d−4p mixing.[22] In such a case, metal 3d−4p mixing is mediated by ligand valence orbital interactions, which allow overlap of both the metal 3d and 4p orbitals. Hence, in a simple picture, one would predict that a short axial ligand along the *z*-axis would allow for a $3d_{z^2}-4p_z$ mixing mechanism. This is consistent with a ligand-based mechanism for metal 3d−4p mixing, which has been previously proposed.[43]

For the Mn(V)-nitrido, the calculations indicate a significant pre-edge feature due to the 1s to $3d_{z^2}$ transition. In the case of the Mn(V)-oxo, the calculations indicate that transitions to both the doubly degenerate d_{xz},d_{yz} orbitals and the d_{z^2} orbital will give rise to significant dipole-allowed intensity (Table 3). This should result in a weaker (d_{xz},d_{yz}) pre-edge peak ~0.7 eV below a more intense (d_{z^2}) pre-edge peak.

Depending on the nature of the p−d mixing, each pre-edge peak is expected to show different polarization characteristics. While dipole-dominant transitions depend only on the $\cos^2\theta$ between the X-ray *e* vector and the absorber−backscatter vector (e_j), the dichroism of quadrupole-dominant transitions is expected to be further complicated due to the additional contribution of the X-ray propagation direction (k_n) to the absorber−backscatter vectors.[37,39,52] In the current case, two Mn(V) compounds showed significantly strong dipole-allowed character, due to 6−9% mixing of metal 4p orbital character into the metal d-based orbitals. Therefore, the $4p-3d_{z^2}$ peak component (6542.9 eV for Mn(V)-nitrido and 6540.16 eV for Mn(V)-oxo) simply follows the trend of the $\cos^2\theta$ dependence (θ, angle between the X-ray *e* vector and the Mn axial ligand vector) as shown in Figure 5. On the other hand, the low-energy $4p-d_{yz,zx}$ component of the Mn(V)-oxo compound (6540.8 eV) shows more complicated polarization character due to a mixture of dipole and quadrupole contribution (Figure 5b).

The Role of High-Valent Mn Species in the OEC. Whether high-valent Mn species are involved in a certain intermediate state of the OEC of PS II has been a key question in understanding the oxygen-evolving mechanism. Widely discussed water oxidation mechanisms catalyzed by the Mn_4Ca cluster include (1) nucleophilic attack by water molecules, (2) oxo-hydroxo fusion, and (3) radical mechanisms. Among these proposed mechanisms, high-valent Mn species such as Mn(V) can potentially play a critical role in the nucleophilic attack mechanism, where either Mn(IV)═O•, Mn(V)═O,[67−69] or Mn(V)≡O species will be formed in the S_4 state.[16,18] Highly electrophilic terminal oxygen could be attacked by a nucleophilic water or hydroxide. Generally, a strong pre-edge peak is considered to be an indicator of a Mn(V) species.[15,33] Such a peak could easily be detected in the tetranuclear cluster, even if Mn(V) only represents 1/4 of the sites. Recently, Haumann et al. studied the Mn *K*-edge spectra during the S_3 to S_4 transition using time-resolved X-ray spectroscopy.[15] Their study showed no intensity changes in the pre-edge peak, and therefore, they concluded the absence of Mn(V) in the S_4 state and that there are no oxidation state or structural changes upon this transition. Whether the intermediate state they detected is really the S_4 state or one state prior to the S_4 state (S_3Y^* state in which a redox-active tyrosine ligand (Yz) that is linked to the OEC is oxidized prior to the metal oxidation (S_4)) has been discussed.[3]

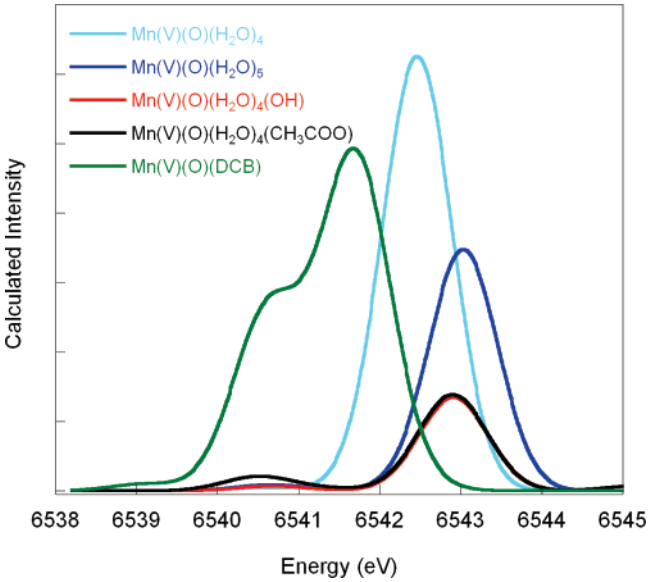

Figure 8. Comparison of the TD-DFT calculated Mn *K*-edge spectra of the Mn(V)-oxo(DCB) as compared to Mn(V)-oxo$(H_2O)_4$, Mn(V)-oxo$(H_2O)_5$, Mn(V)-oxo$(H_2O)_4$(OH), and Mn(V)-oxo$(H_2O)_4(CH_3COO)$. A 1 eV broadening was used for the calculated spectra. A constant shift of 168.2 eV has been applied to all calculated spectra.

Additionally, the following point needs to be considered when the pre-edge intensity is used for an evidence or an absence of the Mn(V) species. The current study shows that the intense pre-edge features in the Mn(V)-nitrido and Mn(V)-oxo complexes result from the short metal−ligand bond, which distorts the complex from an octahedral environment and mediates $3d_{z^2}-4p_z$ mixing. However, it should be noted that the absence of the strong pre-edge peak does not necessarily confirm the absence of Mn(V) species. Mn(V)(TDCPP)(O) porphyrin complexes have been characterized[31] which show significantly reduced pre-edge intensities relative to the complexes discussed here and the related complex previously characterized by Weng et al.[33] The decreased pre-edge intensity in Mn(V)(TDCPP)(O) is attributed to a trans effect due to the presence of a sixth

(66) An experimental estimate for the ratio of dipole to quadrupole transitions is based on polarized studies of D_{2d}- and D_{4h}-$[CuCl_4]^{2-}$. The pre-edge intensity of centrosymmetric D_{4h}-$[CuCl_4]^{2-}$ represents a pure quadrupole-based transition, while the increased intensity in D_{2d}-$[CuCl_4]^{2-}$ represents an additional contribution due to an electric-dipole-allowed transition (ref 42).

(67) It should be noted that a Mn(V)═O species has been proposed by Limburg et al. as an intermediate for their water-oxidizing binuclear Mn complex (refs 68 and 69). Nam and co-workers have also suggested that their Mn(V)-oxo porphyrin complexes have double bond character (ref 31). The present study shows that the calculated bond orders (based on Löwdin analysis) for five-coordinate Mn(V)-oxo species are close to the idealized value of 3.0, while for six-coordinate complexes, the bond order is reduced to ~2.5. This indicates that the Mn(V)-oxo bond is weakened due to the presence of a trans-axial ligand (consistent with previous vibrational data (refs 21 and 31); however, it is still a stronger bonding interaction than a double bond.

(68) Limburg, J.; Vrettos, J. S.; Liable-Sands, L. M.; Rheingold, A. L.; Crabtree, R. H.; Brudvig, G. W. *Science* **1999**, *283*, 1524−1527.
(69) Limburg, J.; Vrettos, J. S.; Chen, H. Y.; de Paula, J. C.; Crabtree, R. H.; Brudvig, G. W. *J. Am. Chem. Soc.* **2001**, *123*, 423−430.

ligand, which results in movement of the Mn atom into the equatorial plan and a longer, weaker Mn(V)-oxo bond.

The contribution of a sixth ligand can be evaluated through calculations on hypothetical five-coordinate Mn(V)-oxo$(H_2O)_4$ and six-coordinate Mn(V)-oxo$(H_2O)_4$(X) complexes (where X is the ligand trans to the oxo and X = H_2O, OH^-, or CH_3COO^-). The TD-DFT calculations on this series are shown in Figure 8. The calculated pre-edge for Mn(V)-oxo(DCB) is given as a reference. Similar to Mn(V)-oxo(DCB), the five-coordinate Mn(V)-oxo$(H_2O)_4$ has a very intense pre-edge feature, which is attributed to the short 1.52 Å Mn-oxo bond and the displacement of the Mn from the equatorial plane (by 0.4 Å (vs 0.6 Å for DCB)). By replacing the DCB macrocycle with four waters, the Mn moves further into the equatorial plane (increasing the equatorial ligand field and thus the pre-edge transition energy). This decreased distortion from the *xy*-plane results in a lower total pre-edge intensity and decreased $4p_{xy}$ mixing, resulting in a single pre-edge feature similar to the Mn(V)-nitrido complex. Upon addition of a trans-axial H_2O, the Mn(V)-oxo bond remains short (1.52 Å) but the Mn moves further into the equatorial plane (~0.3 Å displacement). This results in an increase in the calculated pre-edge energy (due to increased ligand field) and a decrease in pre-edge intensity (by a factor of ~2). Addition of a stronger trans-axial ligand, such as hydroxide or carboxylate, results in a weaker Mn-oxo bond (by ~0.05 Å) and further movement of the Mn into to equatorial plane, decreasing the pre-edge intensity by a factor of ~5 relative to the five-coordinate Mn(V)-oxo$(H_2O)_4$. In addition, the presence of a hydroxide or carboxylate also allows for a small amount of $4p_{x,y}$ mixing due to the presence of a π-interaction with these ligands. It is also of interest to note that the presence of a trans-axial ligand reduces the bond order from 2.97 in the five-coordinate M(V)-oxo$(H_2O)_4$ (based on Löwdin analysis) to 2.51, 2.47, and 2.39 in the Mn(V)-oxo$(H_2O)_5$, Mn(V)-oxo$(H_2O)_4$(OH), and Mn(V)-oxo$(H_2O)_4$(CH_3-CHOO), respectively.

In addition to the presence of a trans-axial ligand, protonation could also result in lengthening of the Mn−O bond and thus decrease the pre-edge intensity. Calculations on a five-coordinate Mn(V)$(OH)(H_2O)_4$ complex show that the pre-edge intensity decreases by almost a factor of 3 relative to the five-coordinate Mn(V)-oxo$(H_2O)_4$. The longer Mn−OH (1.62 vs 1.52 Å for the Mn-oxo) results in a weaker ligand field and a pre-edge transition to ~1 eV lower energy. Such an effect has been observed by Green and co-workers in XAS studies of compound II in chloroperoxidase, where protonation of the ferryl intermediate results in a ~0.2 Å lengthening of the Fe−O bond and a coupled decrease in pre-edge transition energy and intensity.[70,71] However, elongation of the Mn(V)−O bond by protonation is unlikely to be an option in the case of the higher S states of PS II.

The above explanation of the relationship between pre-edge intensity and the Mn−O bond length and coordination environment also extends to Mn(IV), for which one would expect oxo or hydroxo complexes to have a pre-edge at lower energy when compared to analogous Mn(V) species. Hence, the pre-edge spectra can provide complementary information and when coupled to DFT calculations provide insight into reactive intermediates, although caution must be exercised in using the pre-edge spectrum as an isolated signature of oxidation state. Thus, determining whether Mn(IV)═O•, Mn(V)═O, or Mn(V)≡O species are involved in the catalytic mechanism of PS II will also require a detailed understanding of the geometric and electronic structure of the intermediates.

This study has provided the opportunity to evaluate the origins of pre-edge transitions in Mn complexes through polarized XAS studies combined with DFT calculations and adds to the understanding of high-valent Mn species. The extension of this approach to more complex model systems and eventually to the tetramanganese cluster in PS II should enhance our understanding of this complex system and its electronic and geometric structure.

Acknowledgment. This work was supported by the Director, Office of Science, Basic Energy Sciences, Division of Chemical Sciences, Geosciences, and Biosciences of the Department of Energy under Contract DE-AC02-05CH11231 (V.K.Y.), National Institutes of Health (Grant GM 55302, V.K.Y.), and the National Science Foundation (Grant MCB-0342807, E.I.S.). Synchrotron radiation facilities were provided by the Advanced Light Source Berkeley (Contract DE-AC02-05CH11231), and Stanford Synchrotron Radiation Laboratory, operated by the DOE, Office of Basic Energy Sciences. The Structural Molecular Biology program is supported by the National Institutes of Health, National Center for Research Resources, Biomedical Technology Program, and by the Department of Energy, Office of Biological and Environmental Research. We thank Prof. Frank Neese for helpful discussions on the TD-DFT calculations. We are also grateful to Prof. Karl Wieghardt and Dr. Uwe Bergmann for their encouragement and useful discussions. We thank Dr. Matthew Latimer, the SMB group at SSRL, and Dr. Sirine Fakra (ALS) for their help.

Supporting Information Available: Experimental details of XAS and XRD measurements, supporting data on EXAFS of Mn(V)-nitrido and Mn(V)-oxo compounds and angular dependence of the quadrupole-allowed transitions. This material is available free of charge via the Internet at http://pubs.acs.org.

JA071286B

(70) Green, M. T.; Dawson, J. H.; Gray, H. B. *Science* **2004**, *304*, 1653−1656.

(71) Stone, K. L.; Behan, R. K.; Green, M. T. *Proc. Natl. Acad. Sci. U.S.A.* **2005**, *102*, 16563−16565.